PHYSICAL REVIEW B **93**, 214437 (2016)

Spin-wave excitation modes in thick vortex-state circular ferromagnetic nanodots

R. V. Verba,[1,2,*] A. Hierro-Rodriguez,[1] D. Navas,[1] J. Ding,[3] X. M. Liu,[3] A. O. Adeyeye,[3]
K. Y. Guslienko,[4,5] and G. N. Kakazei[1,3]

[1]*IFIMUP-IN/Departamento de Fisica e Astronomia, Universidade do Porto, 4169-007 Porto, Portugal*
[2]*Institute of Magnetism, National Academy of Sciences of Ukraine, Kyiv 03142, Ukraine*
[3]*Information Storage Materials Laboratory, Department of Electrical and Computer Engineering, National University of Singapore, Singapore 117576, Singapore*
[4]*Departamento de Física de Materiales, Universidad del País Vasco, UPV/EHU, 20018 San Sebastián, Spain*
[5]*IKERBASQUE, the Basque Foundation for Science, 48013 Bilbao, Spain*

(Received 1 May 2016; published 28 June 2016)

We study both experimentally and using micromagnetic simulations how the spin excitation spectra of the vortex-state circular dots made of soft magnetic material change with the dot thickness t in the range $t = 20$–80 nm. It is found that in addition to higher-order gyrotropic modes which are nonuniform along the dot thickness and were observed earlier, azimuthal spin-wave modes having curled structure at the dot top and bottom faces appear in the spectrum when increasing the dot thickness. For the dot thickness $t > 50$ nm these "curled" modes become the lowest ones in the spin-wave excitation spectrum. It is also shown that all spin-wave modes with azimuthal index $m = \pm 1$ are hybridized with the vortex gyrotropic modes. However, while "common" azimuthal $(0, \pm 1)$ modes are hybridized with the main gyrotropic G_0 mode and reveal large frequency splitting of their doublet, the curled modes can be hybridized with higher-order gyrotropic modes and the doublet frequency splitting vanishes with the dot thickness increase.

DOI: 10.1103/PhysRevB.93.214437

I. INTRODUCTION

Spin excitation spectra of patterned ferromagnetic films is one of the central topics in modern solid-state magnetism. The spin-wave dispersion relations, i.e., dependence of the excitation frequency on the wave vector, are continuous in bulk magnets and infinite films, and excitation eigenmodes are plane waves with a well-defined wave vector. However, the situation is essentially different for patterned films. The spin excitation frequencies are discrete due to system confinement as was first demonstrated by measuring Brillouin light scattering (BLS) spectra in Refs. [1,2]. The eigenmode profiles are inhomogeneous due to inhomogeneous internal fields even in the case of uniform magnetization ground state. The wave vector is not a good quantum number anymore, and the eigenmodes are classified using integer numbers according to their symmetry and number of nodes of dynamical magnetization in different directions. Calculation of the excitation spectra of patterned films is a complicated problem due to the necessity of accounting simultaneously for short-range exchange and long-range dipolar interactions. Another complication is that the magnetization ground state is often inhomogeneous, e.g., vortex, skyrmion, domain wall, etc. That is a reason why a numerical approach to the problem is justified.

Nowadays there is a new wave of interest in magnetic skyrmions [3], topologically nontrivial vortex-like magnetization configurations in magnetic films, stripes, and dots. It was established very recently that the skyrmions having topological charge 1 can be stabilized in ultrathin multilayer films/dots at room temperature [4,5]. There are Bloch skyrmions resembling magnetic vortices, and Néel skyrmions, stabilized by the Dzyaloshinskii-Moriya interaction (DMI). However, DMI is not obligatory to stabilize Bloch skyrmions; they could be also stabilized by interplay of magnetic anisotropy and magnetostatics [6]. The magnetization dynamics in the presence of a topological soliton (vortex, skyrmion) drastically differ from the uniformly ordered magnets. For instance, the azimuthal spin-wave modes in GHz frequency range and giant soliton mass were detected in vortex [7] and bubble skyrmion dots [8].

The simplest nontrivial magnetization configurations in soft magnetic materials are magnetic vortices. The complicated skyrmion dynamics can be understood studying magnetic vortex dynamics (vortex is a half-skyrmion bearing topological charge 1/2) and extending to skyrmions the excitation mode classification introduced for vortices. The vortex/skyrmion excitation modes are divided in two groups: low-frequency gyrotropic modes, immediately related to the nonzero topological charge, and high-frequency spin-wave modes classified according to their symmetry and number of nodes in the radial (n) and azimuthal (m) directions. The dynamical magnetization components are proportional to $a_n(\rho)\cos(m\phi - \omega t)$, $b_n(\rho)\sin(m\phi - \omega t)$, where ρ,ϕ are the in-plane polar coordinates. The excitation eigenmodes can also be conventionally divided into internal (low frequency) and external (high frequency) modes [9–11]. It is accepted that internal modes are related to weak magnetic soliton deformations and are localized close to the vortex/skyrmion center; they include translation (gyrotropic) and vortex/skyrmion core breathing modes.

The spin excitation spectrum in the presence of the magnetic vortex ground state was investigated in detail in Refs. [12–23]. The spin excitations of the vortex-state submicron ferromagnetic particles (dots, typically of circular or square shape) were measured by Novosad *et al.* using BLS [12]. Then such measurements were conducted using the time-resolved

*Corresponding author: verrv@ukr.net

Kerr effect [13–17], BLS [18,19], ferromagnetic resonance [20,21], and x-ray imaging [22,23]. All these measurements and corresponding theoretical models [24,25] were developed for relatively thin dots (2D case), when the dependence of magnetization on the thickness coordinate can be neglected. For this case the analytical approach to the problem is simplified due to strong pinning of dynamical magnetization at the dot lateral edges [24,26].

It was established that the observed spin excitation spectra of vortex-state thin (thickness is 30 nm and below) circular ferromagnetic dot consist of uniform gyrotropic mode, several frequency doublets of the azimuthal ($m = \pm 1$, any n) spin-wave modes for an in-plane microwave excitation field, or radially symmetric ($m = 0$, any n) spin-wave modes for out-of-plane microwave magnetic field. The question arises: what will be the influence of the third dimension on the dot excitation spectra, when the dots become essentially 3D objects? Recently it was found [27–30] that in thicker circular dots higher-order gyrotropic modes, inhomogeneous along the dot thickness, can be excited. We denote the gyrotropic modes as G_l, according to the number l of nodes of dynamical magnetization along the dot thickness coordinate.

Here we study how the third dimension and existence of these higher-order gyromodes ($l > 0$) changes the high-frequency spin-wave excitation spectra of the dot. Besides enrichment of the spectra caused by coupling of the azimuthal modes with different gyrotropic ones, the significant difference in the intensity between clockwise (negative index m) and counterclockwise (positive index m) modes of the same types was observed. We also found a type of the azimuthal spin-wave modes that can exist solely in thick dots and are beyond the (n,m,l) spin-wave eigenmode classification.

In this article we focus on gyrotropic and spin-wave excitation modes of the vortex ground state of thick cylindrical magnetic dots made of soft magnetic material. The paper is organized as follows. The sample fabrication and the broadband ferromagnetic resonance measurement techniques as well as micromagnetic simulation methods are described in Sec. II. Measured and simulated resonance spectra and micromagnetic profiles of spin-wave modes are presented in Sec. III. The results of simulations and the interpretation of resonance experiments are discussed in Sec. IV. Finally, the conclusions are presented in Sec. V.

II. METHODS

Sample fabrication. Periodic arrays of circular permalloy ($Ni_{80}Fe_{20}$ alloy) dots with diameter $2R = 300$ nm and pitch $p = 620$ nm, which is sufficient to eliminate interdot dipolar interaction, were fabricated on Si substrate over a large area (4×4 mm^2) using deep ultraviolet lithography at 248 nm exposure wavelength followed by electron beam evaporation and liftoff process. Details of the processing steps can be found elsewhere [31]. The thickness t of the $Ni_{80}Fe_{20}$ dots was varied from 20 nm to 80 nm. Even for the large dot aspect ratio thickness/radius ($t/R = 0.53$ for $t = 80$ nm), scanning electron microscopy revealed that the dots are flat circular objects with sharp edges [Fig. 1(a)].

The magnetization behavior of the fabricated dot arrays was characterized using a focused magneto-optical Kerr (MOKE)

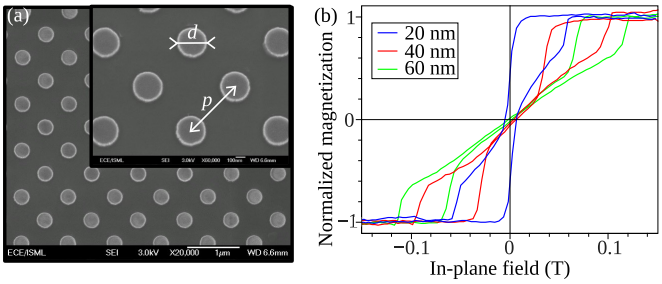

FIG. 1. Scanning electron microscopy image of fabricated dots with 80 nm thickness (a) and measured hysteresis loops of dots with different thickness (b).

setup with a spot size of about 5 μm in the longitudinal geometry. All the measured hysteresis loops, shown in Fig. 1(b), have a double triangle shape and zero remanence, typical for the circular dots with the vortex ground state. As expected, vortex nucleation and annihilation fields are getting larger with dot thickness increase. Nucleation and annihilation processes in all the arrays are quite pronounced, which is clear evidence of the dots' identity inside the array.

Microwave absorption measurements. The microwave absorption spectra of the dot arrays in the symmetric vortex ground state (i.e., in the absence of an external in-plane magnetic field) and at room temperature was measured using a vector network analyzer by sweeping the microwave magnetic field frequency within the 50 MHz to 20 GHz range. Standard short, open, load, through (SOLT) calibration was performed before the high-frequency measurements. The samples were placed face down on top of a 50 ohm coplanar waveguide (CPW) with a length of 6300 μm, width of the signal line of 20 μm, and distance between signal and ground line of 10 μm (see the sketch of the measurements setup in Fig. 2). 5 dBm input microwave power generated ac magnetic field of the magnitude about 2 Oe and 10-time averaging was used to improve the signal/noise ratio. It is important to note that the microwave magnetic field h_{rf} is excited around the signal line. Therefore for dots above the signal line h_{rf} has an in-plane orientation, when for the dots above the gap it has a perpendicular orientation (Fig. 2). The measured microwave absorption spectra are presented in Figs. 3, 5, 7.

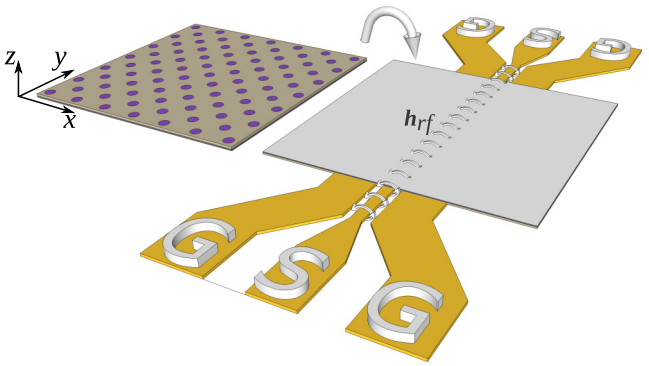

FIG. 2. Schematic diagram of the measurement setup and the field configuration.

Micromagnetic simulations. In order to identify the excitation modes observed experimentally and obtain a deeper insight on the magnetization dynamics in thick vortex-state dots we performed a set of micromagnetic simulations using MuMax3 software [32]. In all simulations the following typical material parameters of permalloy were used [33,34]: saturation magnetization $M_s = 8.1 \times 10^5$ A/m, exchange constant $A_{ex} = 1.05 \times 10^{-11}$ J/m, gyromagnetic ratio $\gamma = 1.86 \times 10^{11}$ rad/(s T), and Gilbert damping constant $\alpha_G = 0.01$. With these parameters, a good agreement was achieved between simulations and experiments except for 20 nm thick dots (see below). Cell size was chosen to be $2.5 \times 2.5 \times 5$ nm^3 (in x, y, z directions, respectively). It was checked that simulations with smaller cell size led to the same results.

To achieve desired accuracy instead of common magnetic field pulse excitation we used single-frequency excitation. For each excitation frequency ω magnetization dynamics was simulated during the time $4/(\alpha_G \omega)$, which is sufficient to reach a stationary state with 98% accuracy, then magnetization dynamics was recorded during several excitation frequency periods. The microwave absorption spectra was calculated as common: $P \sim \omega V_{dot} \mathrm{Im}[\langle \boldsymbol{b}^*(t) \cdot \boldsymbol{m}(t) \rangle]$, where the angle brackets mean averaging over the oscillation period, ω is the excitation frequency, V_{dot} is the dot volume, and $\boldsymbol{b}(t)$ is the microwave magnetic field. In the simulations we used linearly polarized magnetic excitation field of 1 Oe magnitude. To distinguish overlapping resonance peaks, circularly polarized clockwise (CW) and counterclockwise (CCW) microwave excitation fields were also used. The complex excitation mode profiles were calculated as the averaged over several oscillation period value $\boldsymbol{m} = \langle [\boldsymbol{M}(t) - \boldsymbol{M}_0] \exp[-i\omega t] \rangle$, which gives magnetization precession amplitude and phase distribution. In all figures below the real part, $|\boldsymbol{m}| \cos[\phi_z]$, $\phi_z = \arg[m_z]$, of the complex mode profile is presented.

III. MICROWAVE ABSORPTION SPECTRA AND EIGENMODE PROFILES

A. Thin-dot case (t = 20 nm)

Let us consider first the magnetization dynamics of the thinnest dots with the thickness $t = 20$ nm. The spin excitation spectra of thin vortex-state dots are well known [35]; they contain one gyrotropic mode G_0 and a set of spin-wave modes which are characterized by radial and azimuthal indices n and m, respectively (the thickness index is $l = 0$; otherwise the mode frequencies become very high and excitation efficiency negligibly small). An in-plane oscillating magnetic field can excite only modes with the azimuthal number $m = \pm 1$, which are often called "azimuthal" modes. All azimuthal modes are split into doublets; i.e., modes with the azimuthal number $m = +1$ and $m = -1$ have different frequencies, which is a result of the hybridization with the gyrotropic mode [36].

The experimentally measured and micromagnetically simulated absorption spectra for 20 nm thick dots are shown in Fig. 3. Note that in the experiment we were not able to control polarity and chirality of vortices. But the absorption spectra are independent of them for all the samples, as was verified by simulations—only mode structure depends on the vortex

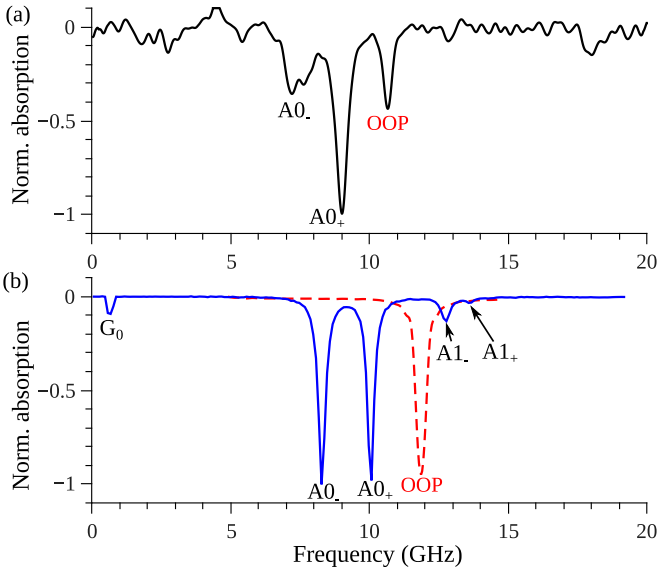

FIG. 3. Experimental (a) and simulated (b) microwave absorption spectra of the circular permalloy dots having 20 nm thickness and 150 nm radius. In (b) blue solid line corresponds to in-plane magnetic excitation field, red dashed to out-of-plane excitation field.

polarity p, but not on the chirality χ. For definiteness we use the value $p = 1$ (magnetization of the vortex core is in the $+z$ direction) for all the simulations presented below.

The lowest gyrotropic mode G_0 having frequency 0.56 GHz (in simulations) is almost invisible in the experimental spectra due to low microwave absorption, which is proportional to the mode frequency. For the considered vortex polarity $p = 1$ the sense of the vortex core gyrotropic rotation in the x-y plane is counterclockwise (CCW) (all mode profiles below will be presented in this way). Below we denote all spin-wave modes propagating in the CCW direction as having the azimuthal index $m = +1$, and the modes propagating in the clockwise (CW) direction as $m = -1$.

In the higher frequency range the simulated spectrum [Fig. 3(b)] contains two clear frequency doublets. These doublets correspond to the azimuthal modes having radial indices $n = 0$ (lower doublet) and $n = 1$ (higher frequency doublet), profiles of which are shown in Fig. 4. For simplicity in the figures and text below we use the following brief notations: the spin-wave modes with $n = 0$, $m = +1, -1$ are denoted as $A0_+$ and $A0_-$, and the modes with $n = 1$, $m = +1, -1$ as $A1_+$ and $A1_-$, respectively. In both doublets the mode, which is counterpropagating to the gyrotropic mode, i.e., CW mode with $m = -1$, has lower frequency in the doublet.

In the experimental spectrum, however, there are three approximately equidistant peaks. To understand the nature of the third peak we simulated microwave absorption spectrum under the out-of-plane (OOP) excitation field. The OOP microwave field excites a different set of spin-wave modes having the azimuthal index $m = 0$. Since our patterned films cover all the stripline, but not only the signal line, the OOP microwave field acts on the dots in the vicinity of the gaps between the signal line and ground (see Fig. 2). Simulations reveal that the OOP field excites the (0,0) mode, which lies above the $A0_+$ mode. Comparing the experimental and simulated spectra it

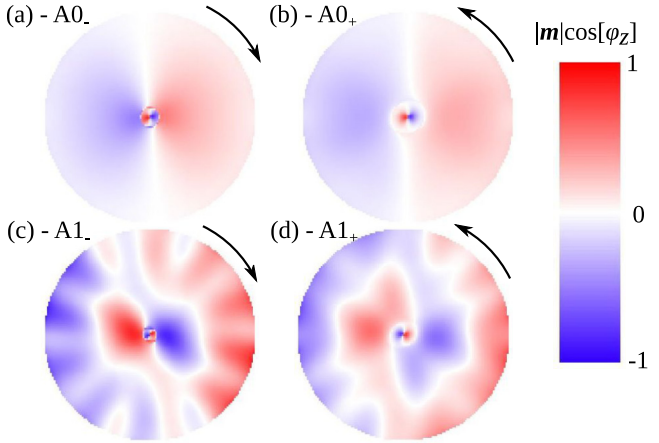

FIG. 4. Azimuthal spin-wave mode profiles in a nanodot having 20 nm thickness. (a) and (b) Zeroth azimuthal modes running in the CW ($A0_-$ mode) and CCW ($A0_+$) directions, respectively. (c) and (d) First azimuthal modes $A1_-$ and $A1_+$. Arrows show the running spin-wave mode direction.

becomes clear that the experimentally observed modes are the $A0_-$, $A0_+$, and (0,0) modes, respectively. Note that the mode peak positions in the experimental spectrum are shifted to the lower-frequency region with respect to the simulated ones. The most probable reason for this is a decrease of the saturation magnetization with respect to the nominal one due to surface effects. With an increase of the dot thickness this effect becomes smaller and, therefore, the measured and simulated absorption peak positions are in better accordance.

B. Intermediate dot thickness ($t = 40$ nm)

The absorption spectra for the dots having $t = 40$ nm thickness are shown in Fig. 5. For these samples in addition to the gyrotropic mode G_0 being uniform along the dot thickness, we also observed the first-order gyrotropic mode (G_1) at 6.85 GHz. The G_1 mode has a node in the central plane of the dot and, similarly to other gyrotropic modes, is running in the CCW direction ($m = +1$) for the considered vortex polarity $p = +1$.

The spectrum of azimuthal modes for 40 nm thick dots also becomes more complex. The lowest in frequency azimuthal modes are still the $A0_-$ and $A0_+$ modes at 8.55 GHz and 11.3 GHz, respectively. Their profiles are almost the same as for the thinnest dots with $t = 20$ nm, which are shown in Figs. 4(a) and 4(b). Namely, these modes are almost uniform along the dot thickness (see Sec. IV C), have no nodes in the radial direction (except in the vortex core region due to the hybridization with gyrotropic mode; see Sec. IV A), and the azimuthal nodal lines are straight except the vortex core region. The doublet of $A0_\pm$ modes has a large frequency splitting, approximately 1 GHz larger than for 20 nm thick dots, in agreement with Ref. [36].

The azimuthal modes $A1_\pm$ with 1 radial node are also visible in the absorption spectra. However, the splitting in their doublet becomes very small, only 100 MHz, and we were able to distinguish these mode frequencies in simulations only using circularly polarized microwave magnetic field to excite

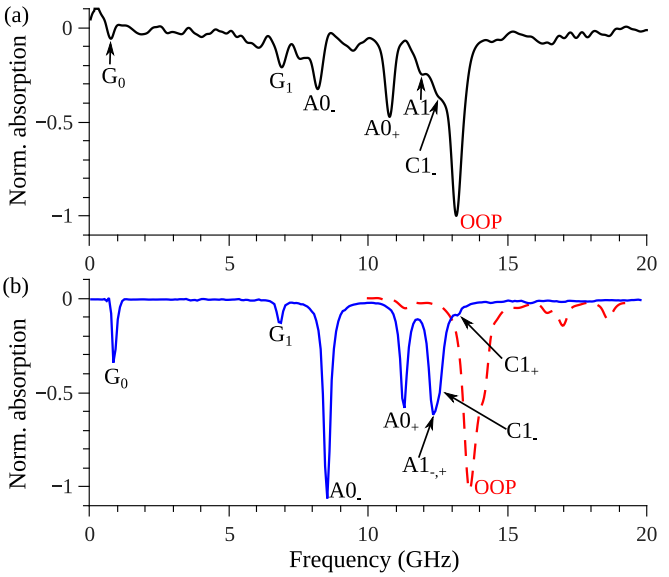

FIG. 5. Experimental (a) and simulated (b) microwave absorption spectra of the dots having 40 nm thickness; in (b) blue solid line corresponds to in-plane magnetic excitation field, red dashed to out-of-plane excitation field.

them separately. As for A0 modes, profiles of $A1_\pm$ modes are similar to ones in the 20 nm thick dots [shown in Figs. 4(c) and 4(d)]. In particular, the azimuthal nodal line in the dot plane is approximately straight and the nodal line in the radial direction is close to circular.

However, besides common A0 and A1 modes we observed another frequency doublet in the simulations at slightly higher frequency, 12.57 GHz and 13.35 GHz, respectively. One mode from this doublet is also clearly distinguishable in the experimental spectrum. Profiles of these modes at the dot faces and central plane are shown in Fig. 6. At every radial position there are 2 nodes moving in the CW or CCW directions, respectively. However, in contrast to "common" A0 and A1 modes, the azimuthal nodal line is not straight anymore and

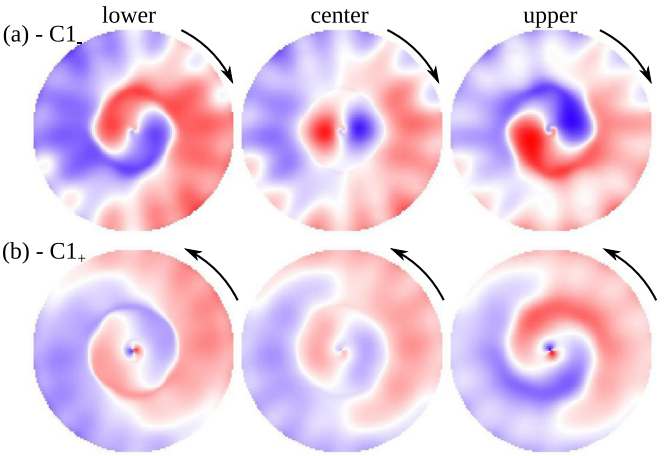

FIG. 6. Dynamical magnetization profiles of the curled azimuthal spin-wave modes $C1_-$ (a) and $C1_+$ (b) in 40 nm thick dot at the lower, central, and upper plane of the dot. Color scale is the same as in Fig. 4.

becomes curled. This curled structure is the most pronounced at the dot faces and, prominently, the direction of the curling is opposite at the top/bottom dot faces. Only in the central plane of the dot there is no curling and the mode profile resembles the common A1 mode. Since the curled structure is the most prominent feature of these spin-wave modes we propose to call them "curled" (C) modes and identify them by the number of the nodes in the radial directions in the dot central plane. Namely, the modes shown in Figs. 6(a) and 6(b) are the $C1_-$ and $C1_+$ modes, respectively. Note that common numeration of curled modes by using 3 indices (radial, azimuthal, and thickness) is impossible; see Sec. IV B, where the nature of curled modes is discussed.

Another prominent feature of C1 modes is that the curling directions for the CW and CCW modes are opposite (see Fig. 6). By micromagnetic simulations we verified that the structure of C1 modes is independent of the vortex chirality χ as for common spin-wave modes of thin vortex-state dots. Reversing the vortex polarity, naturally, leads to the reversing of the curling directions to opposite ones. Note also that for the dot thickness $t = 40$ nm the C1 mode frequencies are close to the A1 mode frequencies and are slightly hybridized with them. The structure of the curled modes will be more clear for the thicker dots described below.

Finally, as for 20 nm thick dots in the experiment we observed the (0,0) spin-wave mode at 13.2 GHz (13.7 GHz in the simulations), which is excited due to the presence of the OOP microwave field in the experimental setup.

C. Thick dots ($t = 60$, 80 nm)

The spin excitation spectra of thicker dots with the thicknesses 60 nm and 80 nm show similar features. For both samples the second-order gyrotropic mode G_2 appears in the absorption spectra, shown in Fig. 7 (for 60 nm the G_2 mode is visible only in the simulations). Also for 80 nm thick dots the nonuniform gyrotropic mode G_1 becomes more intensive than the uniform one (G_0); this effect was discussed in Refs. [27,37].

In the spectrum of azimuthal modes we still observe the doublet of A0 modes with a significant splitting: 2 GHz for $t =$ 60 nm and 2.6 GHz for $t = 80$ nm. Since the spin excitation spectrum becomes denser, A0 modes hybridize or simply overlap with other dot modes, which results in a deviation of their profiles from ideal ones, as for the $A0_+$ mode shown in Fig. 8(a), which is close to the $A1_-$ mode. Nevertheless, the main features of the A0 modes—uniformity along the dot thickness and an approximately straight azimuthal nodal line—remain unchanged. Note also that $A0_\pm$ modes remain the most intensive among all excited spin-wave modes under applied in-plane microwave field, meaning that they have the largest in-plane dynamical magnetic moment.

However, in contrast to thinner dots, the A0 modes are no longer the lowest modes in the spectrum of spin-wave modes with azimuthal number $|m| = 1$. The lowest spin-wave modes are the doublet of the curled modes $C1_-$ and $C1_+$. The peak amplitudes in the doublet are not similar: the $C1_-$ mode has significantly higher peak amplitude; also the frequency splitting in the doublet decreases with the dot thickness. For the considered dot thickness the curled modes C1 have well-defined curled structure at the dot faces and a

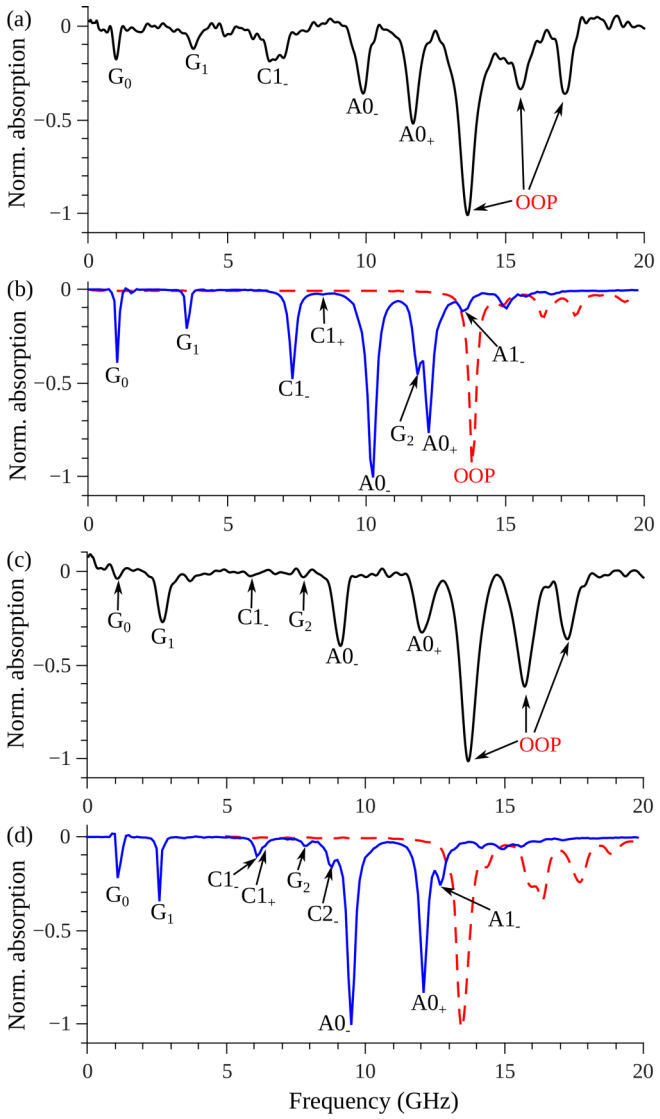

FIG. 7. Microwave absorption spectra of 60 nm thick [(a), (b)] and 80 nm thick [(c), (d)] dots. (a) and (c) Experiment. (b) and (d) Simulations. In (b) and (d), blue solid line corresponds to in-plane magnetic excitation field, red dashed to out-of-plane excitation field.

common profile with one radial node at the dot central plane, which resembles the $A1_\pm$ mode in a thin vortex-state dot [see Figs. 8(b) and 8(c)]. It is also clear from Figs. 8(b) and 8(c) that the $C1_+$ mode is more hybridized with the gyrotropic mode: its amplitude in the vortex core region is significantly higher than in the case of the $C1_-$ mode. The hybridization is discussed in Sec. IV C in more detail.

Besides the A0 and C1 modes we were able to observe the $A1_-$ mode, while the $A1_+$ mode is invisible. Such asymmetry in the excitation efficiency of the CW and CCW azimuthal modes is a general feature of the spin-wave excitation spectra and is discussed below (Sec. IV A).

Also, we found higher-order curled azimuthal modes in the simulations. In particular, for the 80 nm thick dot there are the $C2_-$ mode at 8.8 GHz and $C3_-$ mode at 12 GHz. The last one is not visible in the spectrum shown in Fig. 7(d) due to overlapping with the $A0_+$ mode, but it is clearly

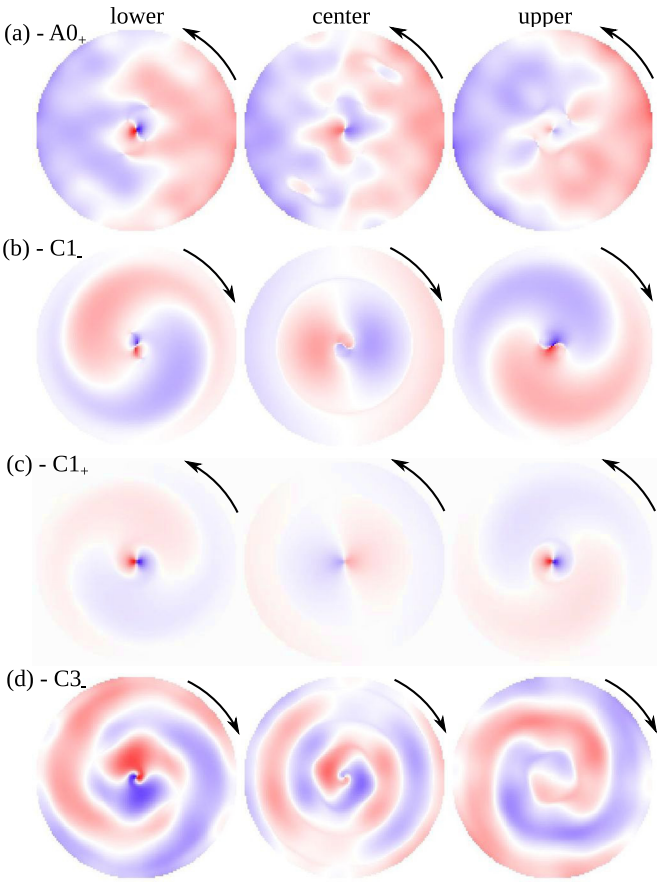

FIG. 8. Profiles of the azimuthal spin-wave modes in 80 nm thick dot at the bottom, central, and top planes of the dot. (a) Zeroth azimuthal mode $A0_+$. (b) and (c) Curled modes $C1_-$ and $C1_+$, respectively. (d) Curled mode $C3_-$. Color scale is the same as in Fig. 4; arrows show the running mode direction.

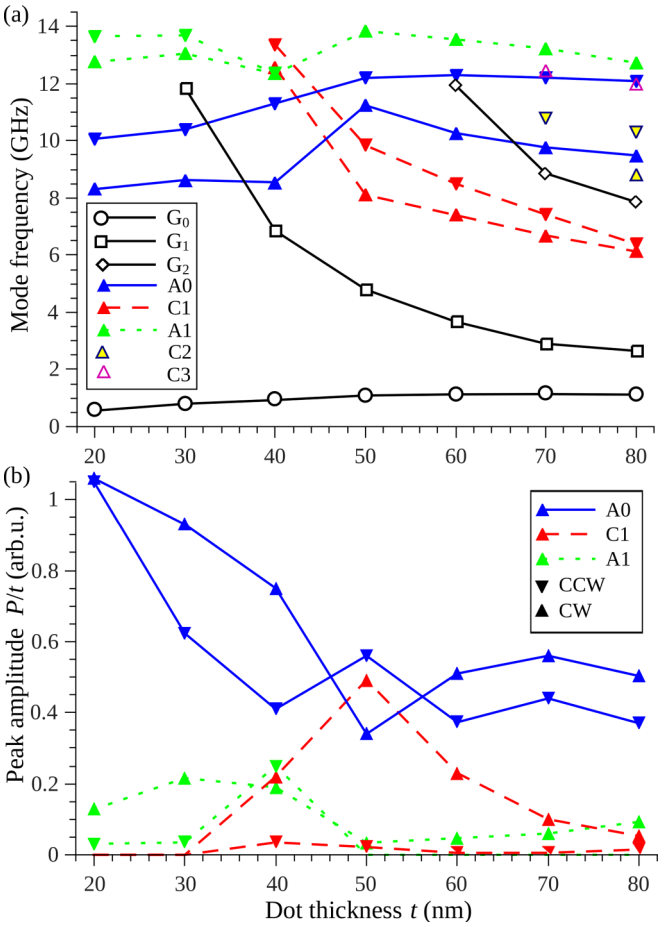

FIG. 9. Dependencies of simulated spin excitation mode frequencies (a) and absorption peak amplitudes, normalized to the dot thickness (b), on the dot thickness t, obtained from micromagnetic simulations; open circles, squares, and diamonds correspond to the gyrotropic modes, up and down triangles to CW ($m = -1$) and CCW ($m = +1$) azimuthal spin-wave modes, respectively.

distinguishable in the spectrum under the CW microwave excitation field. As an example, in Fig. 8(d) the profile of the $C3_-$ mode is shown. Similarly to the C1 modes, higher curled modes have characteristic curling structure at the dot faces, but with more that one node in every radial direction. The directions of curling at the dot faces are opposite. At the dot central plane the profile of the $Cn_\pm$ mode becomes more or less similar to the $(n,m = \pm 1)$ mode of a thin dot. In particular, the $C3_-$ mode shown in Fig. 8(d) has clear $n = 3$ nodes in the radial direction in the dot central plane, therefore it is denoted as the C3 mode.

IV. DISCUSSION

A. Evolution of mode frequencies and excitation efficiency with dot thickness

In order to give a deeper insight on the evolution of spin excitation mode frequencies and absorption peak amplitudes as functions of the dot thickness we simulated additionally the absorption spectra of circular dots with the thicknesses $t = 30$, 50, 70 nm. The simulation results are summarized in Fig. 9. The absorption peak amplitudes in Fig. 9(b) are normalized to the dot thickness t since the absorbed power is proportional to the nanodot volume. The absorption amplitudes were calculated using CW (CCW) excitation field for the modes with $m = -1$ ($m = +1$), as this allows us to determine the resonance peak amplitudes more precisely due to smaller peaks overlapping.

As expected [7], the frequency of the uniform gyrotropic mode G_0 increases with the dot thickness up to $t \approx 70$ nm, and then starts to decrease due to interaction with the azimuthal $An_\pm$ spin-wave modes. Frequencies of the higher-order gyrotropic modes G_1 and G_2, naturally, decrease with the dot thickness increasing as $1/t^2$ due to the exchange contribution.

The frequencies of the azimuthal $A0_\pm$ modes increase with dot thickness first and then seem to saturate. Note that according to [36,38] the frequencies of the An_m modes are proportional to $\sqrt{t/R}$, and the frequency splitting of the $An_\pm$ doublets is proportional to t/R in the limit $t \ll R$. This is not fulfilled anymore because the aspect ratio t/R of the investigated dots is not small, being in the range 0.13–0.53. The splitting in the A0 mode frequency doublet also becomes large in thicker dots. The exception near the dot thickness $t = 50$ nm is related to the intersection and hybridization of A0 modes with C1 modes. Notably, A0 modes are the most

intensive among all spin-wave modes for all the considered dot thicknesses.

The curled modes $C1_{\pm}$ become the lowest ones in the azimuthal mode spectrum for the dot thickness $t > 45$ nm, and their frequencies decrease with the dot thickness increasing in whole thickness range investigated. In general, the intensities of C1 modes are significantly smaller than those of A0 modes due to strongly inhomogeneous mode dynamical magnetization. An exception appears close to the dot thickness $t = 50$ nm, where these modes hybridize with A0 modes. Also, near this point the frequency splitting of the C1 mode doublets is maximal, meaning that this splitting is, mainly, a result of the hybridization with A0 modes which have large frequency splitting. It should be also noted that in the thin-dot case ($t = 20$, 30 nm) we could not find any mode in the microwave absorption spectra, which could be considered as a continuation of the thickness dependence of the C1 mode frequencies. This means that the C1 modes originate from inhomogeneous spin-wave modes of a thin vortex-state dot with zero averaged dynamical magnetic moment.

Figure 9(a) also shows the positions of distinct azimuthal mode peaks, which were not observed systematically in all the simulated samples due to low excitation efficiency. These are curled modes $C2_{-}$ (clearly distinguishable for $t = 80$ nm), $C2_{+}$ ($t = 70$, 80 nm), and $C3_{-}$ (shown for $t = 70$, 80 nm and found also for $t = 50$ nm in a higher frequency range). The C2, C3 mode frequencies are also decreasing with the dot thickness increasing and, similarly to C1 modes, the higher curled modes are expected to become lower in frequency than the most intensive A0 modes at some dot thickness.

From Fig. 9 one can point out two general features. First, in all azimuthal mode doublets, the frequency of the mode running in the opposite to gyrotropic mode direction (CW in our case) is the lower one. While this feature is known for common azimuthal A0, A1 modes [36], here it is shown that curled modes also follow this rule. Also, the azimuthal modes, which are counterpropagating to G_0, are more intensive in the frequency doublets [20]; an exception for A0 modes at $t = 50$ nm is a result of the mode hybridization. In the ultimate case only CW modes of some frequency doublets were found in absorption spectra, as for A1 modes for the dot thickness $t > 50$ nm or C3 modes (see Fig. 9). The reason of this asymmetry is the hybridization of spin-wave modes with the azimuthal index $m = \pm 1$ and the gyrotropic modes. As shown in Ref. [38] for the thin-dot case and clearly visible in Figs. 4(c), 4(d), and 6, the hybridization leads to the appearance of an additional radial node near the vortex core boundary for the CCW azimuthal modes, and no nodes appear in the case of CW modes, counterpropagating to the G_0 mode. That is, the hybridization decreases the dynamic magnetic moment of the CCW modes and, consequently, their coupling to the spatially uniform excitation magnetic field.

B. Curled modes

Let us now discuss features of the curled azimuthal modes. As we pointed out earlier, one of their prominent features is the asymmetry of the mode profiles at the dot faces, at which the directions of the mode magnetization curling are opposite. It is clear that such profiles cannot be parametrized as $m_\alpha(\boldsymbol{r}) = f_1(\rho) f_2(\phi) f_3(z)$, while this parametrization is approximately valid for all spin-wave modes in the thin-dot case [24,39], as well as for the A0 and A1 modes in the studied thick dots. For example, the thickness profile of the C1 modes changes from almost uniform to antisymmetric depending on the azimuthal angle. Indeed, if for the spin-wave modes shown in Figs. 8(b) and 8(c) one build the x-z (horizontal) cross section through the dot center, the corresponding mode profiles will be almost constant along the thickness coordinate z [these profiles are shown in Figs. 11(c) and 11(d) below]. However, in the perpendicular y-z (vertical) cross section the profiles are definitely antisymmetric: dynamic magnetization has opposite sign at the dot faces.

Such features are unexpected for the well-studied case of quasi-two-dimensional static magnetization distributions, e.g., for a thin vortex-state dot. However, the vortex ground state in thick dots is no longer quasi-two-dimensional. As an illustration, in Fig. 10 we plot the static magnetization distribution at the dot faces for the 80 nm thick dot. These distributions are not similar anymore to the common Usov-Peschany vortex ansatz [40]: near the vortex core (but not within the core) the magnetization distribution deviates from ideal one $\boldsymbol{M}(\boldsymbol{r}) = \chi M_s \boldsymbol{e}_\phi$ and a nonzero positive (negative) radial M_ρ component of the magnetization appears at the upper (lower) dot surfaces. Only in the central dot plane the magnetization component $M_\rho = 0$. That is, $M_\rho(\rho, z)$ is an odd function of the thickness coordinate z. The appearance of the ρ component is a consequence of static demagnetization fields produced by the vortex core magnetization. The maximal value of the M_ρ component depends, naturally, on the dot thickness: while for the thickness $t = 20$ nm $M_\rho < 0.1 M_s$, for $t = 80$ nm the maximal value is $M_{\rho,\max} = 0.34 M_s$. A bubble-skyrmion magnetization distribution similar to that presented in Fig. 8 was simulated by Moutafis *et al.* [41] for thick FePt dots with strong perpendicular anisotropy. In our case of soft magnetic material, the magnetization configuration shown in Fig. 8 corresponds to an equilibrium balance of the exchange and magnetostatic energies. Another peculiarity of the magnetization configuration of the thick dot (not shown in Fig. 8) is barrel-like vortex core shape with the core radius $R_c(z)$ being minimal at the dot faces $z = \pm t/2$ [42].

Since the static magnetization configuration is not uniform along the dot thickness, the appearance of nonsymmetric

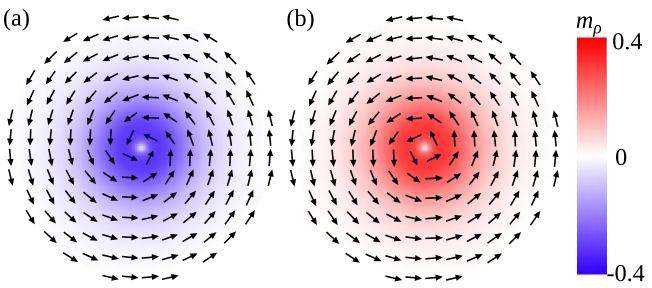

FIG. 10. Static magnetization distribution in 80 nm thick nanodot at the bottom (a) and top (b) dot faces; color scale depicts the distribution of the normalized $m_\rho = M_\rho / M_s$ magnetization component.

spin-wave modes with a complex structure, like the curled modes, becomes natural. It also becomes clear why there are no peaks in the absorption spectra of thin dots, which could be considered as a continuation of C1 mode frequencies. These modes originate from modes with nonuniform along the dot thickness dynamical magnetization and having zero excitation efficiency by a spatially uniform microwave field; recall that the thickness profile of the C1 modes at some instant azimuthal position is antisymmetric. The modifications of thickness modes and hybridization with A0 modes, which makes the resulting C1 modes visible in the absorption spectra, become possible due to the change of the static magnetization configuration when the dot thickness increases.

Finally, an interesting point is why C1 modes become the lowest-frequency spin-wave modes with the azimuthal number $m = \pm 1$. In a thin dot A0 modes propagate in the direction of the local static magnetization $\boldsymbol{M} = \chi M_s \boldsymbol{e}_\phi$, which leads to a decrease of spin-wave mode frequency similarly to the well-known backward-volume magnetostatic waves in ferromagnetic films [43]. But, as was shown above, in thicker vortex-state dots the direction e_ϕ, in which A0 modes propagate, is no longer the direction of the local static magnetization in all the out-of-core regions of a dot. Instead of this, the curled structure of C1 modes allows them to follow the local magnetization direction in a thick dot, which makes the C1 mode frequencies the lowest in the spin-wave excitation mode spectra. Of course, more rigorous explanation requires an analytical calculation and lies beyond the scope of this article.

C. Hybridization of azimuthal and gyrotropic modes

Finally, let us briefly consider the hybridization of the azimuthal modes with gyrotropic modes. As was pointed earlier, this hybridization takes place for all the azimuthal modes and has a result that the azimuthal modes, counterpropagating to gyrotropic modes, becomes lower in frequency and more intensive in the doublet. However, the question is with which of the gyrotropic modes does the hybridization occur?

The simplest way to answer this question is to look on the thickness profiles of azimuthal modes, which are shown in Fig. 11; namely, calculate the number of nodes of the mode magnetization in the vortex core region. From this figure it is clear that $A0_\pm$ modes are always hybridized with the uniform gyrotropic mode G_0. It could seem that there is an exception for the $A0_+$ mode for the dot thickness $t = 60$ nm, but in this case the $A0_+$ mode is simply close to the G_2 mode and the appearance of 2 nodes in the vortex core region is the result of simple mode overlapping, but not a hybridization. The hybridization with the uniform G_0 gyrotropic mode results in a high-frequency splitting of the A0 mode doublets.

In contrast, the behavior of the C1 modes is different. While the $C1_-$ mode, which is counterpropagating to gyrotropic modes, is hybridized with the G_0 mode for all the dot thicknesses [Fig. 11(c)], the $C1_+$ mode is hybridized with different gyrotropic modes depending on the dot thickness. For $t = 40$ nm, it is hybridized with a superposition of G_0 and G_1 modes (profile has one not clear node in the vortex core region); for $t = 60$ nm, with the G_1 mode (1 clear node); and for the case $t = 80$ nm, the hybridization occurs with the G_2 mode

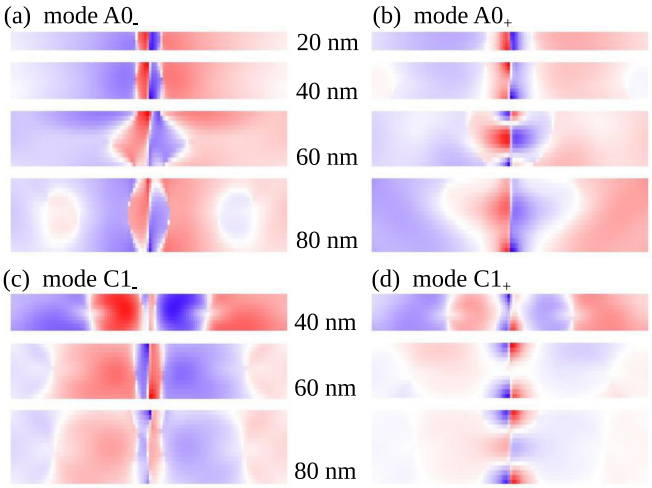

FIG. 11. Profiles of the dynamical magnetization of the azimuthal spin-wave modes across the dot thickness. (a) Zeroth azimuthal mode $A0_-$. (b) Mode $A0_+$. (c) and (d) Curled modes $C1_-$ and $C1_+$, respectively. Color scale is the same as in Fig. 4.

[Fig. 11(d)]. The hybridization with higher-order gyrotropic modes is the reason why the splitting of the C1 mode frequency doublet decreases with the dot thickness, since the overlapping integral, to which the splitting is proportional [36], is lower for the modes inhomogeneous over the dot thickness [44].

This uncommon behavior of C1 modes could be understood by recalling that the degree of the mode hybridization (i) is proportional to the dynamic overlapping of modes, i.e., to the overlapping of the effective dynamic field created by one mode with the profile of another mode, and (ii) inversely depends on the difference of mode eigenfrequencies [36,45]. Note that when considering mode hybridization using common complex amplitude formalism it is necessary to take into account "physical" modes with positive frequencies, as well as their complex conjugated mirrors having negative frequencies [45] (more details about "physical" and "formal conjugated" modes can be found in Refs. [45,46]).

A0 modes are almost uniform along the dot thickness; consequently, their overlapping is maximal with the G_0 mode. In contrast, due to a complex structure, C1 modes could overlap with higher-order gyrotropic modes. Thus, the intermode distance becomes also an important factor for the determination of the mode hybridization. For the $C1_+$ mode the closest gyrotropic mode with the same sense of rotation (CCW) is different for different dot thickness: for $t < 60$ nm it is the G_1 mode, and for thicker dots, the G_2 mode [see Fig. 9(a)]. That is why the mode hybridization changes with the dot thickness. In contrast, the $C1_-$ mode, propagating in the CW direction, cannot overlap with "physical" gyrotropic modes: CW and CCW modes are orthogonal. Instead, the $C1_-$ mode overlaps with "formal conjugated" gyrotropic modes having negative frequency and CW "propagation" direction. The conjugated gyrotropic mode, which is the closest to the C1 modes, is the G_0 mode for *any* dot thickness, as it has the minimal absolute value of frequency. That is why the $C1_-$ mode is always hybridized with the G_0 mode, as observed in the simulations.

V. SUMMARY

In this work we presented an experimental and micromagnetic study of the spin-wave excitation spectra of thick vortex-state ferromagnetic dots. It is found that an increased dot thickness not only leads to the appearance of higher-order gyrotropic modes, but also modifies the azimuthal spin-wave mode spectrum, in which additional "curled" modes appear. The curled modes have characteristic curled structure at the top and bottom dot surfaces with opposite curling direction at them, and resemble common $(n, \pm 1)$ azimuthal modes at the dot central plane. Due to their complex structure the curled modes cannot be characterized by radial, azimuthal, and thickness indices as all other spin-wave modes. Instead, they could be characterized by the number of radial nodes at the dot central plane. We observed several curled modes, up to third-order curled mode C3 in the 80 nm thick dots.

The curled spin-wave modes originate from higher-order thickness modes of thin vortex-state dots and their appearance is directly related to the deviation of static magnetization configuration from quasi-two-dimensional with the dot thickness increasing. The frequencies of the curled modes depend inversely on the dot thickness and, in particular, for $t > 50$ nm C1 modes become the lowest among the azimuthal modes. Due to a complex nonuniform structure the curled modes have small excitation efficiency by uniform microwave magnetic field, and the most intensive azimuthal modes are $A0_{\pm}$ modes.

All the azimuthal modes of a thick vortex-state dot are hybridized with gyrotropic modes and their frequencies are split into doublets due to this hybridization. In the doublets of curled modes, as for all the azimuthal modes, the mode which is counterpropagating to the gyrotropic mode has lower frequency and higher excitation efficiency. However, while A0 modes have large splitting in the doublet and are hybridized with the G_0 mode for all studied dot thicknesses, the splitting of $C1_{\pm}$ modes becomes vanishing at high dot thicknesses. Moreover, C1 modes in the doublet are hybridized with different gyrotropic modes: the mode $C1_{-}$, which is counterpropagating to the G_n mode, is always hybridized with the G_0 mode, while the copropagating $C1_{+}$ mode is hybridized with the G_0, G_1, and G_2 modes depending on the dot thickness, which is a result of the interplay of mode dynamic magnetization overlapping and intermode distance.

ACKNOWLEDGMENTS

Work at IFIMUP was supported by the Portuguese Foundation of Science and Technology (FCT) through Projects No. EXPL/IF/00981/2013 and No. EXPL/IF/01191/2013, the "Investigador FCT" program (D.N. and G.N.K.), Grant No. SFRH/BPD/90471/2012, and POPH/FSE programs (A.H.R.). Work at IMag was supported by the Ministry of Education and Science of Ukraine (Project No. 0115U002716). Work at NUS was supported by the National Research Foundation, Prime Minister's Office, Singapore, under its Competitive Research Programme (CRP Award No. NRF-CRP 10-2012-03). A.O.A. is a member of the Singapore Spintronics Consortium (SG-SPIN). R.V.V. and K.Y.G. acknowledge funding from the European Union Horizon 2020 research and innovation program under Marie Skłodowska-Curie Grant Agreement No. 644348. K.Y.G. acknowledges support by IKERBASQUE (the Basque Foundation for Science) and Spanish MINECO Grant No. MAT2013-47078-C2-1-P. The authors would like to thank Dr. N. Singh from A*Star Institute of Microelectronics, Singapore, for his help with template fabrication.

[1] C. Mathieu, C. Hartmann, M. Bauer, O. Buettner, S. Riedling, B. Roos, S. O. Demokritov, B. Hillebrands, B. Bartenlian, C. Chappert, D. Decanini, F. Rousseaux, E. Cambril, A. Müller, B. Hoffmann, and U. Hartmann, Appl. Phys. Lett. **70**, 2912 (1997).

[2] C. Mathieu, J. Jorzick, A. Frank, S. O. Demokritov, A. N. Slavin, B. Hillebrands, B. Bartenlian, C. Chappert, D. Decanini, F. Rousseaux, and E. Cambril, Phys. Rev. Lett. **81**, 3968 (1998).

[3] A. Fert, V. Cros, and J. Sampaio, Nat. Nanotechnol. **8**, 152 (2013).

[4] C. Moreau-Luchaire, C. Moutafis, N. Reyren, J. Sampaio, C. A. F. Vaz, N. Van Horne, K. Bouzehouane, K. Garcia, C. Deranlot, P. Warnicke, P. Wohlhüter, J.-M. George, M. Weigand, J. Raabe, V. Cros, and A. Fert, Nat. Nanotechnol. **11**, 444 (2016).

[5] O. Boulle, J. Vogel, H. Yang, S. Pizzini, D. de Souza Chaves, A. Locatelli, T. O. Menteş, A. Sala, L. D. Buda-Prejbeanu, O. Klein, M. Belmeguenai, Y. Roussigné, A. Stashkevich, S. M. Chérif, L. Aballe, M. Foerster, M. Chshiev, S. Auffret, I. M. Miron, and G. Gaudin, Nat. Nanotechnol. **11**, 449 (2016).

[6] K. Guslienko, IEEE Magn. Lett. **6**, 4000104 (2015).

[7] K. Y. Guslienko, G. N. Kakazei, J. Ding, X. M. Liu, and A. O. Adeyeye, Sci. Rep. **5**, 13881 (2015).

[8] F. Buttner, C. Moutafis, M. Schneider, B. Kruger, C. M. Gunther, J. Geilhufe, C. v. K. Schmising, J. Mohanty, B. Pfau, S. Schaffert, A. Bisig, M. Foerster, T. Schulz, C. A. F. Vaz, J. H. Franken, H. J. M. Swagten, M. Klaui, and S. Eisebitt, Nat. Phys. **11**, 225 (2015).

[9] B. A. Ivanov, H. J. Schnitzer, F. G. Mertens, and G. M. Wysin, Phys. Rev. B **58**, 8464 (1998).

[10] D. D. Sheka, I. A. Yastremsky, B. A. Ivanov, G. M. Wysin, and F. G. Mertens, Phys. Rev. B **69**, 054429 (2004).

[11] V. Novosad, F. Y. Fradin, P. E. Roy, K. S. Buchanan, K. Y. Guslienko, and S. D. Bader, Phys. Rev. B **72**, 024455 (2005).

[12] V. Novosad, M. Grimsditch, K. Y. Guslienko, P. Vavassori, Y. Otani, and S. D. Bader, Phys. Rev. B **66**, 052407 (2002).

[13] J. P. Park, P. Eames, D. M. Engebretson, J. Berezovsky, and P. A. Crowell, Phys. Rev. B **67**, 020403 (2003).

[14] J. P. Park and P. A. Crowell, Phys. Rev. Lett. **95**, 167201 (2005).

[15] X. Zhu, Z. Liu, V. Metlushko, P. Grütter, and M. R. Freeman, Phys. Rev. B **71**, 180408 (2005).

[16] M. Buess, T. P. J. Knowles, R. Höllinger, T. Haug, U. Krey, D. Weiss, D. Pescia, M. R. Scheinfein, and C. H. Back, Phys. Rev. B **71**, 104415 (2005).

[17] F. Hoffmann, G. Woltersdorf, K. Perzlmaier, A. N. Slavin, V. S. Tiberkevich, A. Bischof, D. Weiss, and C. H. Back, Phys. Rev. B **76**, 014416 (2007).
[18] L. Giovannini, F. Montoncello, F. Nizzoli, G. Gubbiotti, G. Carlotti, T. Okuno, T. Shinjo, and M. Grimsditch, Phys. Rev. B **70**, 172404 (2004).
[19] K. Vogt, O. Sukhostavets, H. Schultheiss, B. Obry, P. Pirro, A. A. Serga, T. Sebastian, J. Gonzalez, K. Y. Guslienko, and B. Hillebrands, Phys. Rev. B **84**, 174401 (2011).
[20] F. G. Aliev, J. F. Sierra, A. A. Awad, G. N. Kakazei, D.-S. Han, S.-K. Kim, V. Metlushko, B. Ilic, and K. Y. Guslienko, Phys. Rev. B **79**, 174433 (2009).
[21] A. A. Awad, K. Y. Guslienko, J. F. Sierra, G. N. Kakazei, V. Metlushko, and F. G. Aliev, Appl. Phys. Lett. **96**, 012503 (2010).
[22] S.-B. Choe, Y. Acremann, A. Scholl, A. Bauer, A. Doran, J. Stöhr, and H. A. Padmore, Science **304**, 420 (2004).
[23] K. Y. Guslienko, X. F. Han, D. J. Keavney, R. Divan, and S. D. Bader, Phys. Rev. Lett. **96**, 067205 (2006).
[24] K. Y. Guslienko, W. Scholz, R. W. Chantrell, and V. Novosad, Phys. Rev. B **71**, 144407 (2005).
[25] R. Zivieri and F. Nizzoli, Phys. Rev. B **78**, 064418 (2008).
[26] K. Y. Guslienko and A. N. Slavin, Phys. Rev. B **72**, 014463 (2005).
[27] J. Ding, G. N. Kakazei, X. Liu, K. Y. Guslienko, and A. O. Adeyeye, Sci. Rep. **4**, 4796 (2014).
[28] V. S. Pribiag, I. N. Krivorotov, G. D. Fuchs, P. M. Braganca, O. Ozatay, J. C. Sankey, D. C. Ralph, and R. A. Buhrman, Nat. Phys. **3**, 498 (2007).
[29] M. Yan, R. Hertel, and C. M. Schneider, Phys. Rev. B **76**, 094407 (2007).
[30] R. Zarzuela, E. M. Chudnovsky, and J. Tejada, Phys. Rev. B **87**, 014413 (2013).
[31] A. O. Adeyeye and N. Singh, J. Phys. D: Appl. Phys. **41**, 153001 (2008).
[32] A. Vansteenkiste, J. Leliaert, M. Dvornik, M. Helsen, F. Garcia-Sanchez, and B. Van Waeyenberge, AIP Adv. **4**, 107133 (2014).
[33] G. Nahrwold, J. M. Scholtyssek, S. Motl-Ziegler, O. Albrecht, U. Merkt, and G. Meier, J. Appl. Phys. **108**, 013907 (2010).
[34] N. Smith, D. Markham, and D. La Tourette, J. Appl. Phys. **65**, 4362 (1989).
[35] K. Y. Guslienko, J. Nanosci. Nanotechnol. **8**, 2745 (2008).
[36] K. Y. Guslienko, A. N. Slavin, V. Tiberkevich, and S.-K. Kim, Phys. Rev. Lett. **101**, 247203 (2008).
[37] J. Ding, G. N. Kakazei, X. M. Liu, K. Y. Guslienko, and A. O. Adeyeye, Appl. Phys. Lett. **104**, 192405 (2014).
[38] K. Y. Guslienko, G. R. Aranda, and J. M. Gonzalez, Phys. Rev. B **81**, 014414 (2010).
[39] B. A. Ivanov and C. E. Zaspel, Phys. Rev. Lett. **94**, 027205 (2005).
[40] N. Usov and S. Peschany, J. Magn. Magn. Mater. **118**, L290 (1993).
[41] C. Moutafis, S. Komineas, C. A. F. Vaz, J. A. C. Bland, T. Shima, T. Seki, and K. Takanashi, Phys. Rev. B **76**, 104426 (2007).
[42] F. Boust and N. Vukadinovic, Phys. Rev. B **70**, 172408 (2004).
[43] A. G. Gurevich and G. A. Melkov, *Magnetization Oscillations and Waves* (CRC Press, New York, 1996), p. 464.
[44] M. Noske, H. Stoll, M. Fähnle, A. Gangwar, G. Woltersdorf, A. Slavin, M. Weigand, G. Dieterle, J. Förster, C. H. Back, and G. Schütz, arXiv:1505.01148.
[45] R. V. Verba, Ukrainian J. Phys. **58**, 758 (2013).
[46] R. Verba, G. Melkov, V. Tiberkevich, and A. Slavin, Phys. Rev. B **85**, 014427 (2012).